

Low-Voltage Aberration-Corrected Transmission Electron Microscopy: Progressing Carbon Nanostructures

F. Börrnert, A. Bachmatiuk, B. Büchner and M. H. Rummeli

Leibniz-Institut für Festkörper- und Werkstoffforschung Dresden e. V., PF 270116, 01171 Dresden, Germany

Carbon nanostructures are regarded as promising building blocks for future electronics. The molecular structure and dynamics of carbon nanostructures is much discussed throughout the literature, mostly from the theoretical side because of a lack of suitable experimental techniques to adequately engage the problem. A technique that has recently become available is low-voltage aberration-corrected transmission electron microscopy. It is a valuable tool with which to directly observe the atomic structure and dynamics of the specimen *in situ*. We demonstrate the use of this technique with different examples from studies dealing with the characterization of molecular junctions in carbon nanostructures and the self-repairing of defects in single-wall carbon nanotubes.

Keywords low-voltage TEM; carbon nanostructures

1. Carbon nanostructures: the motivation for research

Carbon nanostructures are well recognized potential building blocks for future nano-devices [1]. For detailed information on the extraordinary physical properties of the different carbon allotropes that lead to their potential use in applications there are numerous reviews throughout the literature and in this book series.

Assemblies of or defects in such ordered systems can both introduce and destroy properties attractive for applications, so they are the object of vivid research [2]. The defect structure and dynamics of carbon nanostructures is much discussed, mostly from the theoretical side because of a lack of suitable experimental techniques to adequately engage this issue.

A technique that has recently become available is low-voltage aberration-corrected transmission electron microscopy (LV-AC-TEM). In particular, time series of LV-AC-TEM is a valuable tool to directly observe the atomic structure and dynamics of the specimen *in situ*. During irradiation with 80 kV (or lower energy) electrons a perfect lattice of sp^2 carbon is stable. The reduction of the electron energy compared to electron energies in conventional high resolution TEM results in a loss of resolving power needed to sufficiently characterize the specimen structure. The means to regain the necessary resolution is the correction of the spherical aberration of the microscope's objective lens. The advent of spherical aberration lens correctors now makes high resolution low voltage TEM a reality.

Here, we demonstrate the use of LV-AC-TEM with different examples from recent studies dealing with the characterization of molecular junctions in carbon nanostructures and the self-repairing of defects in SWCNTs [3,4].

2. Low-voltage aberration-corrected transmission electron microscopy

The transmission electron microscope (TEM) is an instrument that uses accelerated electrons to produce magnified images of small objects. The basic design of a TEM roughly matches the design of the first light microscopes back in the late 16th century. A source is followed by a beam shaping lens, the condenser, then the beam illuminates the sample, after that another lens, the objective, forms an image of the sample, and, finally, a lens magnifies the image.

The key parameter of a microscope is not the magnification, but the resolution, i. e. the minimum distance two points that can be distinguished from each other are allowed to have. Theoretically, the maximum resolving power of any microscope is in the order of the wave length of the imaging entity, in our case the electrons. The wavelength of accelerated electrons is plotted in Figure 1. The acceleration voltage range shown in Figure 1 matches the voltages commonly used in TEMs. Due to lens aberrations [see paragraph 2.2] the actual resolution that can be reached is more than two orders of magnitude poorer than the theoretical value.

As one can see in figure 1, one only needs to increase the energy of the electrons to resolve smaller structures. The problem with increasing the electron accelerating voltage is that already at medium voltages, which are used in conventional high resolution TEMs, the electrons deposit enough energy into the sample to rapidly destroy fragile objects such as carbon nanostructures.

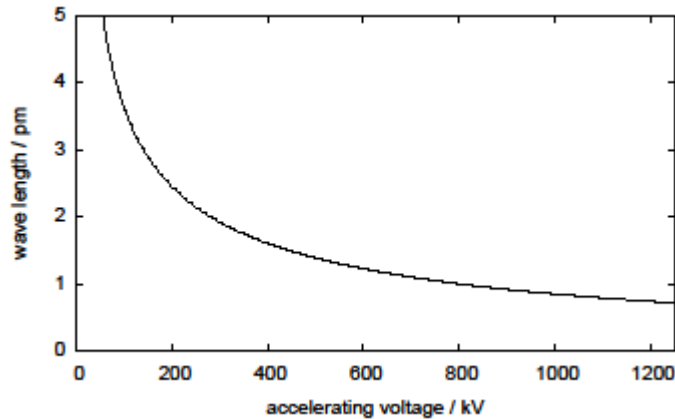


Fig. 1 Wave length of accelerated electrons with respect to the accelerating voltage.

2.1 Low-voltage TEM

The issue of destroying carbon nanostructures very quickly has been addressed theoretically by Smith and co-workers [5]. They calculated a minimum incident electron energy of 86 keV is required to remove a carbon atom from the sp^2 lattice by a knock-on collision. Additionally, defects in the lattice, adherent dirt, and stress (e. g. curvature) lower this threshold. Various studies have confirmed the general trend of the theoretical predictions [6]. Therefore, there is a huge advantage in using acceleration low voltages of 80 kV or even lower when investigating carbon nanostructures.

The drawback of lowering the acceleration voltage is the loss of resolution. If we want to investigate the structure of sp^2 lattices, we need a resolution of at least 0.2 nm, for studying the structure and dynamics of defects *in situ*. A better resolution than that is of even greater value. Unfortunately, the resolution needed can only be reached with acceleration voltages of 200 kV or more in conventional TEMs. The limitation of resolving power in conventional TEMs is predominantly due to the spherical aberration of the objective lens. When one wants to measure samples with low accelerating voltages, the only way to regain a sufficient resolution is to correct the spherical aberration of the objective lens.

2.2 Aberration-corrected TEM

Aberrations are an inherent property of lenses. Simply the fact that a real lens is not infinitely thin introduces aberrations. There are various types of aberrations, but the main resolution-limiting aberration in our case is spherical aberration and is illustrated in Figure 2.

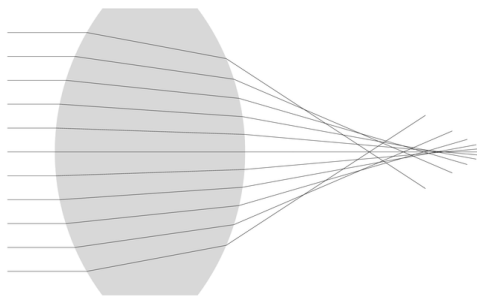


Fig. 2 Schematic illustration of spherical aberration. The parallel rays coming from the left should all meet (focus) at one point on the right side using an ideal non-aberrated lens.

In light optics, since the 1870s, aberrations of a lens can be corrected through additional lenses. For electron optics this was not possible until very recently, because there is no electromagnetic equivalent to a scattering lens for electrons. The first fully operational corrector for the third-order spherical aberration was demonstrated in 1997 [7] based on an idea from 1947 [8] consisting of a complicated system of multipoles and lenses. It has been commercially available for about a decade now.

The use of an aberration corrector improves the point resolution of a TEM by a factor of about two. A state-of-the-art aberration-corrected TEM can have a point resolution of 0.19 nm at an acceleration voltage of 80 kV [9]. These parameters enable a TEM to observe the structure and dynamics of defects in sp^2 carbon lattices *in situ*. For a further enhancement of the resolving power one needs to correct other types of aberrations and improve the electrical and mechanical stability of the instrument. The improvement in terms of lower radiation damage and higher resolution is demonstrated in Figure 3.

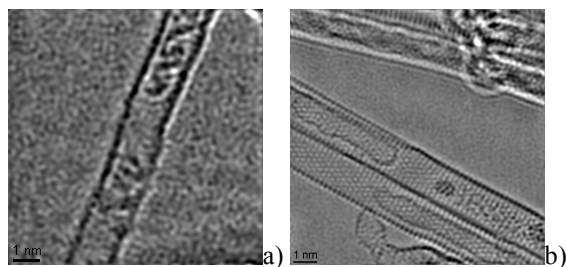


Fig. 3 Comparison between micrographs of the same sample taken with a) conventional high-resolution TEM taken with a FEI Tecnai F30 at 300 kV acceleration voltage, and b) low-voltage aberration-corrected TEM taken with a FEI Titan³ 80-300 with a spherical-aberration corrector for the objective lens at 80 kV acceleration voltage.

In both micrographs of Figure 3 the same sample of single-wall carbon nanotubes is imaged. Figure 3a) has been acquired with a conventional uncorrected high-resolution TEM at a medium acceleration voltage of 300 kV. Figure 3b) was taken by means of LV-AC-TEM. In frame a) the walls of the tubes are already very damaged, whereas in frame b) the tubes remain in perfect shape. In contrast to frame a), in frame b) the crystalline structure of the nanotube is clearly resolved.

3. Application examples to carbon nanostructures

3.1 Experimental

The SWCNTs employed were produced by a laser ablation route and have a mean diameter of ca. 1.5 nm [10]. They were first annealed in air at 380 °C for 0.5 h. A fraction of the tubes were then filled with [6,6]-phenyl-C₆₁-butyric-acid-methyl-ester (PCBM) [11] by annealing them in the presence of PCBM in a sealed quartz ampule with an internal pressure of 10⁻³ Pa at 550 °C for 5 days. For imaging, the sample was drop coated onto standard lacey carbon TEM grid.

An FEI Titan³ 80–300 transmission electron microscope with a CEOS aberration corrector for the objective lens, operating at an acceleration voltage of 80 kV, equipped with a Gatan UltraScan 1000 camera was used. All studies were conducted at room temperature. During a time series an image was taken every 5 seconds with an acquisition time of 0.5 s and all images were compiled into motion pictures. The contrast of the micrographs was enhanced through Fourier filtering by cutting frequencies beyond the information limit of the microscope.

The chirality of the SWNTs was determined by analyzing the Fourier transformed TEM images and measuring the corrected SWNT diameter [see Appendix A.2]. Simulations of the imaging process were obtained using JEMS electron microscopy software [12]. For comparison, noise was added to the simulated images and the same Fourier filtering applied as for the TEM images.

3.2 First example: Single-wall-carbon-nanotube/single-carbon-chain molecular junctions

In the design of nano-electronic devices, a key issue is the fabrication of metal–semiconductor junctions. A single molecular junction between a single carbon chain (SCC) and a single wall carbon nanotube (SWCNT) could provide an attractive solution. Whether a SWCNT is semiconducting or metallic is controlled either through its chirality or through doping [13,14]. Infinite SCCs are semiconducting due to Peierls distortion [15]. However, short SCCs are usually treated as metallic in the literature. Single carbon chains have previously been observed [16-18].

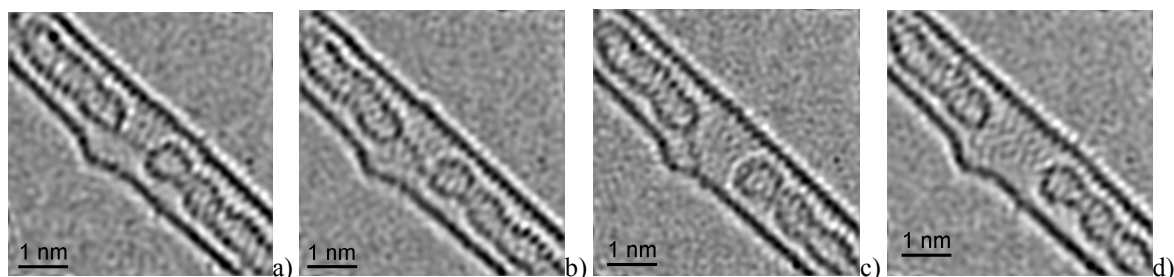


Fig. 4 In situ study showing the dynamics of a SCC bridging two SWCNTs inside a host tube. a) SCC bridging the two inner tubes. b) the attachment point of the SCC to the upper tube has changed. c) The chain disconnects from the lower inner tube. The two inner tubes drift apart, and d) the SCC disappears and the inner tube sections drift further apart. The time elapsed from image a) to d) is 30 s.

In figure 4a) the capped ends from two inner SWCNTs with a chain bridging them can be seen. The host SWCNT features a distortion in the wall structure. The inner SWCNTs were formed earlier *via* the coalescence of PCBM fullerenes driven by the electron beam. In figure 4b), the chain binding the two inner tubes appears to have altered its position. This apparent change in the attachment point could be due to the chain anchor point being mobile or the upper inner tube has rotated. However, the rotation argument is unlikely, because in figure 4c) the attachment point of the chain to the upper inner tube has again changed, yet the upper inner tube structure remained. In frame c) one can also observe that the chain has now disconnected from the lower inner tube and the spacing between the two inner tubes has clearly augmented, suggesting the SCC may have been under strain. The detached end of the chain is seen to have found a new anchor point at the hump-like feature on the host tube. In figure 4d) the two inner SWCNTs have drifted apart further and the carbon chain has disappeared. The hump-like structure on the host tube appears slightly larger suggesting the carbon chain has been absorbed within it. However, it may be possible that part or all of the carbon chain was ejected from the host tube altogether.

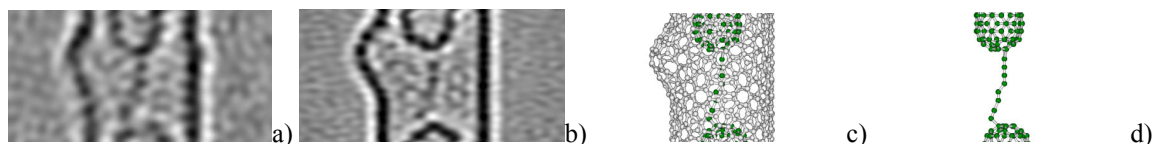


Fig. 5 Comparison of original and simulation of a TEM image of the SWCNT/SCC molecular junction using molecular models. a) Fourier filtered TEM image [cut from figure 4b)], b) Fourier filtered output of a multi-slice simulation of the imaging process, c) ball-and-stick illustration of the underlying molecular model for the simulation, and d) of the inner part of the model to highlight the single carbon chain.

To better comprehend the carbon chain bridging the two SWCNTs within a host tube we generated various simulations of the structure imaging process, see figure 5. A section of the structure from the original micrograph is provided in frame a). In frame b) we present the result of an imaging simulation which matches the original image. The complete underlying ball-and-stick structure is provided in panel c) from which one can see where regions of strong contrast originate. In panel d) the ball-and-stick structure of the carbon chain bridging the two SWCNTs without the host tube is presented. The chirality of the host tube is (14,8). Whilst one cannot conclusively determine the chirality of the inner SWCNT since they are probably still rearranging their structure; our best fit is a (5,5) for both tubes. The carbon chain length is 8 atoms.

Infrared absorption studies on PCBM filled SWCNTs annealed under dynamic ultra-high vacuum conditions at 1500 K show no C–H vibrations confirming cumulene structures are likely, as opposed to alkane chain or polyacetylene type structures. In addition, the stability of the SWCNT/SCC molecular junction we observed was high; it withstood the energy input of the electron beam for over 30 s. Compared to other carbon structures under similar conditions, this value is remarkably high [6]. This stability indicates the carbon chain is most probably entirely formed from carbon atoms as the incorporation of an O or H atom would make it more unstable.

3.3 Second example: *In situ* observations of self-repairing single-wall carbon nanotubes

The mechanism on how carbon nanotubes retain their general structure under irradiation is usually described in terms of material loss and subsequent surface reconstruction [19,20]. However, material ejection has not been shown yet.

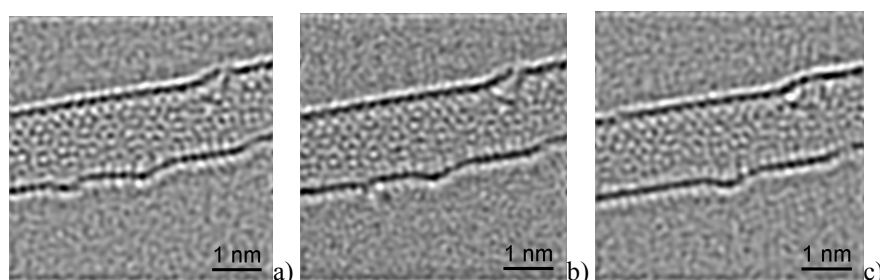


Fig. 6 *In situ* TEM observation of material ejection from a SWCNT. a) study showing the dynamics of a SCC bridging two SWCNTs inside a host tube. a) Hump-like defect in the wall, b) formation of a protrusion, and c) defect has disappeared. The time elapsed between each frame is 5 s.

In Figure 6, frames a)–c) show a series of TEM images of a SWCNT with defects. The time span between each frame is 5 s. In frame a) there is a hump-like defect in the wall of the tube. The chirality of the tube was determined to be (14,9), see Appendix A.2. Frame b) features a dark spot outside the wall at the same position. The hump-like feature has now shrunk significantly. In frame c) there is no longer any defect. The dark spot in the micrograph shows material bound to the wall for a nominal time span, *viz.* the cameras acquisition time.

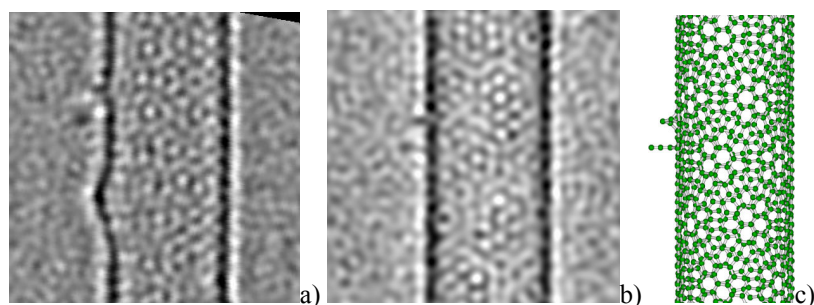


Fig. 7 Comparison of original and simulation of a TEM image of the protrusion. a) Fourier filtered TEM image [cut from figure 6b)], b) Fourier filtered output of a multi-slice simulation of the imaging process of a (14,9) tube with two three-atom protrusions, and c) ball-and-stick illustration of the underlying molecular model for the simulation.

Simulations of the imaging process [see Fig. 7] reveal that this protrusion comprises three carbon atoms. The feature beneath the chain like protrusion can be modelled by a three-atom agglomeration as shown in the ball-and-stick model of Figure 7c). We performed various imaging simulations with different configurations of the underlying model that had varying numbers of atoms in the defect. For these simulations the recording parameters from the original micrographs were used. The simulation study indicates that a protrusion containing less than three atoms cannot be observed in the vicinity of the wall. Protrusions with more than three atoms show a significantly larger footprint than that observed in the micrographs. The formation of three-atom protrusions agrees well with a mechanism proposed by Tsetseris and Pantelides [24] where they studied the stability of self-interstitial structures on graphene and SWCNTs using first-principle calculations. They show that C agglomeration is energetically favourable and that three-atom complexes heal out to very mobile protrusions. In our image series the protrusion vanishes in the last frame, leaving a straight wall. Two possible explanations for the protrusions disappearance are conceivable: either the protrusion becomes mobile on the surface and is incorporated into other defects in the wall or it is ejected from the tube. The latter argument is more probable because if the protrusion were mobile it could not be imaged. Calculations in a previous study of ours show that a carbon chain is not mobile on such a surface [3]. This was due to the weak delocalization of the double bonds in the lattice of the tube. For the present case this is not valid because a very short protrusion with a free end can change the bond orientation easily. With increasing length the chain's mobility is likely to decrease. Our findings are in agreement with previous studies in which the ejection of material from the wall of a SWCNT to produce an undisturbed lattice has been proposed [19,20].

3.4 Third example: Healing of holes in the nanotube wall

Calculations suggest the formation of big holes is unfavourable as compared to multiple small vacancies and that network reconstruction is more efficient in small-diameter nanotubes [21]. However, network reconstruction in nanotubes has been observed in large-diameter multi-wall carbon nanotubes through the interaction of the different walls [22,23].

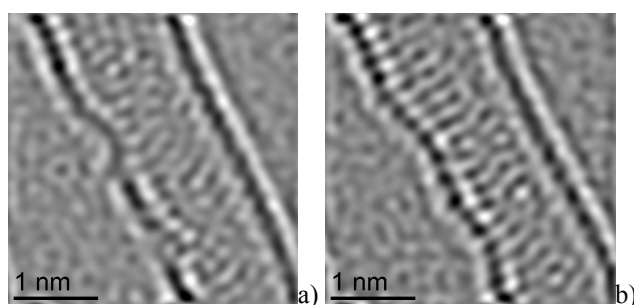


Fig. 8 TEM images showing the closing of two holes in a SWCNT wall. a) Initial state, b) the holes are closed after 20 s.

Two holes can be seen in the wall of a SWCNT in figure 8a). Image simulations allow us to estimate about 20 atoms are missing in the upper hole. Remarkably, these holes then close up over a period of 20 s [see panel b)]. We find no evidence that the holes have rotated or moved elsewhere along the tube. The appearance of new defects in the vicinity of the healing region might be due to the extensive rearrangement of the crystal structure to regain an overall hexagonal lattice. In this case the electron beam provides the energy for the reconstruction of the sp^2 lattice. Heat might lead to similar processes because it is known from optical spectroscopy studies that annealing CNTs leads to an enhanced crystallinity. Previous theoretical studies have shown small holes up to six missing atoms can heal in a (10,10) nanotube with a diameter of 1.4 nm in elevated temperatures [21]. Our observations suggest the healing process is capable of

sealing significantly larger holes than previously shown and display the need for systematic studies of the maximum ratio of defect size and nanotube diameter.

4. Summary

The low-voltage aberration-corrected transmission electron microscope has been demonstrated to be a valuable tool for the investigation of the dynamics of carbon nanostructures *in situ*. It has shown that the high spatial and temporal resolution of this technique allow to follow the evolution of 8-atom carbon chains or 3-atom protrusions attached to carbon nanotubes. Important experimental checks of theoretical models on the atomic scale like the material loss of carbon nanotubes during irradiation and the healing of holes in the nanotube wall are achieved.

A. Appendix

A.1 Fourier filtering of micrographs

Fourier filtering is not only a method for noise suppression and contrast enhancement, but removes possible higher order imaging artefacts.

A bandpass mask is applied to the Fourier transformed micrograph (FTM) in a way that frequencies beyond the information limit of the microscope due to the energy spread of the electrons in the beam are cut to suppress noise. Due to this treatment no information contained in the images is lost, moreover, higher order artefacts due to the image formation process in TEM is removed. Additionally, the very central spot in the FTM is cut to remove large-area illumination gradients. This can be done without information loss because at these low frequencies TEM does not deliver interpretable information due to the phase contrast transfer function becoming zero.

A.2 Determination of the chirality of a SWCNT

The chirality of a SWCNT can be determined by measuring the diameter and the chiral angle of the tube. When measuring the diameter of a tube one has to bear in mind that due to defocus the apparent diameter may be deviating from the real diameter. This should be checked by imaging simulations. To obtain the chiral angle one measures the distance of the respective reflexes of the rolled-up graphene lattice in the FTM to the main axis perpendicular to the original nanotube axis. Because of the symmetry of the FTM it is often more accurate to measure the doubled distance to the mirrored reflex. All reflexes must lie on a circle of $2.13^{-1} \text{ \AA}^{-1}$, due to the bending of the graphene lattice in a tube, the reflexes are line-shaped. The radius of this circle, the main axis in the FTM, and the measured distance now form a right-angled triangle from which one gets the desired angle. The error of the determined angle gets smaller the nearer the reflexes are to the main axis in the FTM, however, the reflex intensity gets rapidly smaller.

Acknowledgements F. B. acknowledges the DFG (RU 1540/8-1), A. B. the Alexander von Humboldt Foundation, and M. H. R. the EU (ECMP) and the Freistaat Sachsen.

References

- [1] Avouris P. Molecular Electronics with Carbon Nanotubes. *Acc. Chem. Res.* 2002;35:1026-1034.
- [2] Charlier J-C. Defects in Carbon Nanotubes. *Acc. Chem. Res.* 2002;35:1063-1069.
- [3] Börmert F, Börmert C, Gorantla S, Liu X, Bachmatiuk A, Joswig J-O, Wagner FR, Schäffel F, Warner JH, Schönfelder R, Rellinghaus B, Gemming T, Thomas J, Knupfer M, Büchner B, Rümmeli MH. Single-wall-carbon-nanotube/single-carbon-chain molecular junctions. *Phys. Rev. B.* 2010;81:085439.
- [4] Börmert F, Gorantla S, Bachmatiuk A, Warner JH, Ibrahim I, Thomas J, Gemming T, Eckert J, Cuniberti G, Büchner B, Rümmeli MH. In situ observations of self-repairing single-walled carbon nanotubes. *Phys. Rev. B.* 2010;81:201401(R).
- [5] Smith BW, Luzzi DE. Electron irradiation effects in single wall carbon nanotubes. *J. Appl. Phys.* 2001;90:3509-3515.
- [6] Warner JH, Schäffel F, Zhong G, Rümmeli MH, Büchner B, Robertson J, Briggs GAD. Investigating the Diameter-Dependent Stability of Single-Walled Carbon Nanotubes. *ACS Nano.* 2009;3:1557-1563.
- [7] Haider M, Rose H, Uhlemann S, Kabius B, Urban K. Towards 0.1 nm resolution with the first spherically corrected transmission electron microscope. *J. Electr. Mic.* 1998;47:395-405.
- [8] Scherzer O. Sphärische und chromatische Korrektur von Elektronenlinsen. *Optik.* 1947;2:114-132.
- [9] Barthel J, Thust A. Quantification of the Information Limit of Transmission Electron Microscopes. *Phys. Rev. Lett.* 2008;101:200801.
- [10] Rümmeli MH, Kramberger C, Löffler M, Jost O, Bystrzejewski M, Grüneis A, Gemming T, Pompe W, Büchner B, Pichler T. Catalyst Volume to Surface Area Constraints for Nucleating Carbon Nanotubes. *J. Phys. Chem. B.* 2007;111:8234-8241.
- [11] Hummelen JC, Knight BW, LePeq F, Wudl F, Yao J, Wilkins CL. Preparation and Characterization of Fulleroid and Methanofullerene Derivatives. *J. Org. Chem.* 1995;60:532-538.

- [12] Stadelmann PA. EMS - A software package for electron diffraction analysis and HREM image simulation in materials science. *Ultramicroscopy*. 1987;21:131-146.
- [13] Kazaoui S, Minami N, Jacquemin R, Kataura H, Achiba Y. Amphoteric doping of single-wall carbon-nanotube thin films as probed by optical absorption spectroscopy. *Phys. Rev. B*. 1999;60:13339-13342.
- [14] Latil S, Roche S, Mayou D, Charlier J-C. Mesoscopic Transport in Chemically Doped Carbon Nanotubes. *Phys. Rev. Lett.* 2004;92:256805.
- [15] Abdurahman A, Shukla A, Dolg M. Ab initio many-body calculations on infinite carbon and boron-nitrogen chains. *Phys. Rev. B*. 2002;65:115106.
- [16] Troiani HE, Miki-Yoshida M, Camacho-Bragado GA, Marques MAL, Rubio A, Ascencio JA, Jose-Yacaman M. Direct Observation of the Mechanical Properties of Single-Walled Carbon Nanotubes and Their Junctions at the Atomic Level. *Nano Lett.* 2003;3:751-755.
- [17] Yuzvinsky TD, Mickelson W, Aloni S, Begtrup GE, Kis A, Zettl A. Shrinking a Carbon Nanotube. *Nano Lett.* 2006;6:2718-2722.
- [18] Jin C, Lan H, Peng L, Suenaga K, Iijima S. Deriving Carbon Atomic Chains from Graphene. *Phys. Rev. Lett.* 2009;102:205501.
- [19] Ajayan PM, Ravikumar V, Charlier J-C. Surface Reconstructions and Dimensional Changes in Single-Walled Carbon Nanotubes. *Phys. Rev. Lett.* 1998;81:1437-1440.
- [20] Ding F, Jiao K, Lin Y, Yakobson BI. How Evaporating Carbon Nanotubes Retain Their Perfection? *Nano Lett.* 2007;7:681-684.
- [21] Kotakoski J, Krasheninnikov AV, Nordlund K. Energetics, structure, and long-range interaction of vacancy-type defects in carbon nanotubes: Atomistic simulations. *Phys. Rev. B*. 2006;74:245420.
- [22] Huang JY, Ding F, Yakobson BI. Vacancy-hole and vacancy-tube migration in multiwall carbon nanotubes. *Phys. Rev. B*. 2008;78:155436.
- [23] Jin C, Suenaga K, Iijima S. Vacancy Migrations in Carbon Nanotubes. *Nano Lett.* 2008;8:1127-1130.
- [24] Tsetseris L, Pantelides ST. Adatom complexes and self-healing mechanisms on graphene and single-wall carbon nanotubes. *Carbon*. 2009;47:901-908.